Planetary and Space Science 248 (2024) 105925

Contents lists available at ScienceDirect

Planetary and Space Science

journal homepage: www.elsevier.com/locate/pss

Spectral ratioing of $Af\rho$ to constrain the dust particle size distribution of comets

Nico Haslebacher [a,*], Nicolas Thomas [a], Raphael Marschall [b]

[a] Physikalisches Institut, University of Bern, Bern, Switzerland
[b] CNRS, Observatoire de la Côte d'Azur, Laboratoire J.-L. Lagrange, Nice, France

ARTICLE INFO

Keywords:
Afrho
Size distribution
Dust coma
Comets

ABSTRACT

A numerical model of cometary dust environments is used to gain a deeper understanding of the relationship between the brightness ($Af\rho$) and the dust particle size distribution in the coma. Specifically, the spectral ratio of $Af\rho$(425 nm)/ $Af\rho$(900 nm) is modelled for a wide range of parameters and tied to the power-law index. The studied parameters are dust composition, terminal outflow velocity and the dust production rate day–night asymmetry. We find that the spectral ratio of $Af\rho$ modelled at 425 nm and 900 nm correlates with the power-law index of the particle size distribution. This method could be used to place constraints on the dust size distributions of comets and as a result improve the use of $Af\rho$ as a proxy for cometary activity. Optically red dust indicates that the scattering is dominated by large particles.

1. Introduction

As comets get closer to perihelion in the inner solar system, sublimation occurs and the gas drags dust particles with it. The resulting gas and dust comae around the nucleus can be seen in ground-based observations even though the nucleus itself is typically only a few kilometres in size. The majority of the light observed by a ground-based observer in broad-band visible wavelengths is sunlight scattered by the dust particles in the coma.

The brightness of a cometary coma can be quantified by $Af\rho$. The $Af\rho$ quantity was introduced by A'Hearn et al. (1984) to provide a measure of the scattered solar radiation by a cometary coma in order to compare measurements taken of different comets and under differing geometrical conditions. Because the original definition of $Af\rho$ is complex, a more precise definition of $Af\rho = Q_{sca}pf\rho$ can be used as discussed by Fink and Rubin (2012). The difference to the original definition is that the albedo A is replaced by the product of the scattering efficiency Q_{sca} and the phase function p of the dust particle. The filling factor f is given by the ratio of the total geometric cross section of the dust particles seen within the aperture to the area of the aperture $\pi\rho^2$, where ρ is the radius of aperture. For isotropic force-free radial outflow, the column density of the dust along a line of sight drops with ρ^{-1}, which means that $Af\rho$ is independent of ρ. For many comets the independence of $Af\rho$ to the aperture is a valid first order approximation (e.g. Thomas and Keller, 1990; Baum et al., 1992), but as discussed by Betzler et al. (2023) the comparison between measurements acquired with different aperture radii should be treated with caution, because $Af\rho$ can be strongly dependent on the aperture radius (also see Jewitt and Meech, 1987; Mazzotta Epifani et al., 2014; Garcia et al., 2020). Because $Af\rho$ correlates with the number of dust particles in the coma it has been used to estimate the activity of comets as described by Weiler et al. (2003). In a later study by Fink and Rubin (2012) it was found that the relationship of the mass loss rate to $Af\rho$ is strongly dependent upon the particle size distribution. Tubiana et al. (2015) showed that relating coma brightness to the dust production rate produces large uncertainties if the particle size distribution is unknown. It was also illustrated by Marschall et al. (2022) that $Af\rho$ on its own is a poor predictor of the dust production rate, but that it can be estimated to within one order of magnitude if the dust size distribution is known. In spite of the issues that the $Af\rho$ formalism has, $Af\rho$ is still commonly used as a proxy for the activity of comets (e.g. Mazzotta Epifani et al., 2007; Sárneczky et al., 2016; Bernardinelli et al., 2021; Betzler et al., 2023). In quantitative conversions of $Af\rho$ to dust mass production rates (as done by Mazzotta Epifani et al., 2014; Garcia et al., 2020) the results are more dependent on the assumptions about the dust than the aperture.

The poor constraints on both particle size distribution and dust densities in the coma are not only limiting our knowledge of remotely observed comets, but also lead to large uncertainties in the dust hazard assessment for cometary fly-by missions (see Marschall et al., 2022). One example is ESA's Comet Interceptor mission (Snodgrass and Jones, 2019; Jones et al., 2024) that aims to fly-by a dynamically new comet,

* Corresponding author.
E-mail address: nico.haslebacher@unibe.ch (N. Haslebacher).

https://doi.org/10.1016/j.pss.2024.105925
Received 13 March 2024; Received in revised form 23 May 2024; Accepted 5 June 2024
Available online 7 June 2024

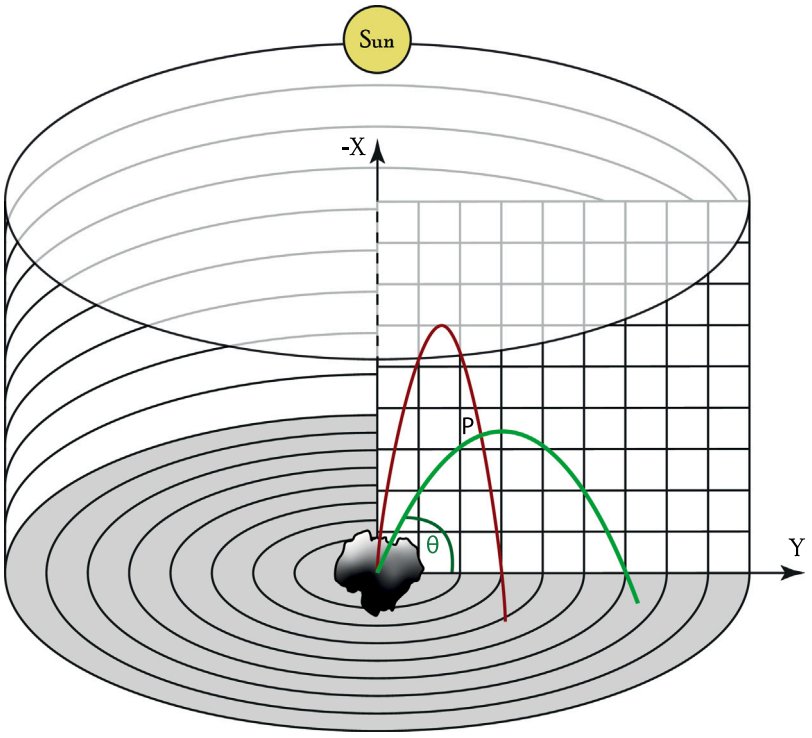

Fig. 1. Cylindrical grid as used in the numerical model. The red and green lines show an example the reflected and direct trajectories of dust particles at point P, where θ is the emission angle (here shown for the particles on direct trajectories). The -X direction is towards the sun.

long period comet, or interstellar object for the first time. In the case of Comet Interceptor the constraining of the dust environment is even more challenging, because the target object is not yet known. Dust particle impacts have been studied during previous missions such as McDonnell et al. (1987), Curdt and Keller (1990), Reinhard (1997), Hörz et al. (2006) and Deep Impact (A'Hearn et al., 2008). By modelling dust particle impacts during a cometary flyby, it was shown by Haslebacher et al. (2022) that the impacts can cause significant perturbations in the attitude of a 3-axis stabilized spacecraft over a wide range of dust production rates depending upon the fly-by velocity and geometry.

Spectroscopic observations of comets have been commonly used to obtain gas composition information in cometary comae (e.g. Lara et al., 2001; Bockelée-Morvan et al., 2004; Langland-Shula and Smith, 2011) and the colour of cometary dust (e.g. Jewitt and Meech, 1986; Lin et al., 2012; Ott et al., 2017). Further, in situ 2 μm–5 μm spectroscopic observations acquired by Virtis-H onboard Rosetta have been used by Bockelée-Morvan et al. (2017) to constrain the power-law index of the particle size distribution. The colour slope of the dust coma was previously linked to the power-law index for comet 29P/Schwassmann–Wachmann 1 and comet C/2016 M1 by Voitko et al. (2022, 2024).

In this work, we study the wavelength dependence of $Af\rho$ and its relationship to the particle size distribution by using a numerical model to estimate $Af\rho$ at different wavelengths for a wide range of parameters. We show that measuring $Af\rho$ for different wavelengths can be used to constrain the dust size distribution under certain assumptions. Specifically, the relationship between the spectral ratio of $Af\rho$ measured at 425 nm and at 900 nm to the power-law index of the particle size distribution is derived for a wide range of boundary conditions. The goal of this work is to enable rough estimations of the particle size distributions of comets. Further, with better constraints on the size distributions the use of $Af\rho$ as a proxy for the activity of comets can be improved.

For signal to noise reasons, the two wavelengths were chosen to be in the visible and near-infrared light. Additionally, a wide separation between the two wavelengths is beneficial. The specific wavelengths were chosen such that prominent gas emission lines such as C_2, C_3, CH or CN (see Sivaraman et al., 1988; Moreels et al., 1988; Cambianica et al., 2021; Lisse et al., 2005) could be avoided as much as possible. Further, the spectral response of modern CCD or CMOS detectors is wide enough to allow for the usage of one single detector for the measurement in both selected wavelengths (see Jorden et al., 2017; Shugarov, 2020). We note that, apart from possible signal to noise issues, our modelling can be adjusted to allow for the use of any two wavelengths to constrain the dust size distribution.

2. Methods

By using a numerical model of cometary dust environments it is possible to model the expected $Af\rho$ for a large range of different parameters. To optimize the running time we use a force-free radial outflow model in addition to our full numerical model. We note that the importance of running time optimizations is due to the large number of particle size bins necessary to make accurate calculations. Further, we want to be able to re-run our model for specific use cases in a reasonable time frame. In summary we use the following two models:

- a numerical model considering both solar radiation pressure (which means reflected particles) and a day–night asymmetry,
- an isotropic force-free radial outflow model.

In Figs. 3–5 we show that the isotropic force-free radial outflow provides a good approximation in the context of this work compared to the numerical model.

2.1. Assumptions

The assumptions made to keep our models simple and time-efficient are explained below.

The coma is assumed to follow cylindrical symmetry, which makes it possible to calculate the trajectories of the dust particles on a two-dimensional grid (see Fig. 1). We note that this assumption is only

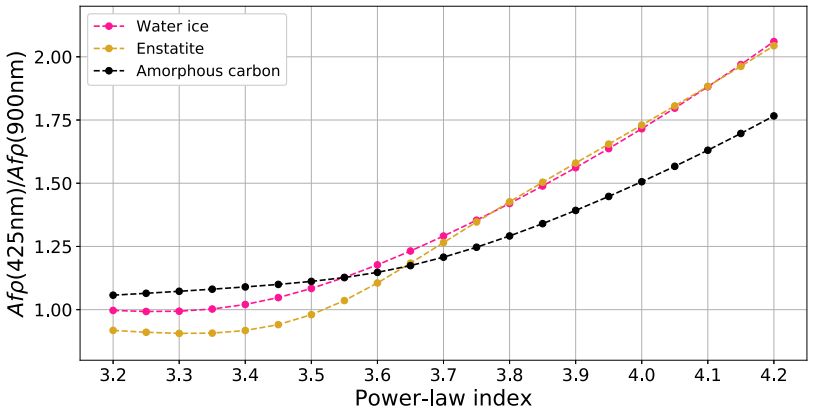

Fig. 2. Spectral ratio of $Af\rho$ in relation to the power-law index for three different dust compositions. The parameters related to the outflow velocity are set as Q_g = 7000 kg s^{-1}, R_N = 4000 m, T_N = 310 K and ρ_d = 800 kg m^{-3}.

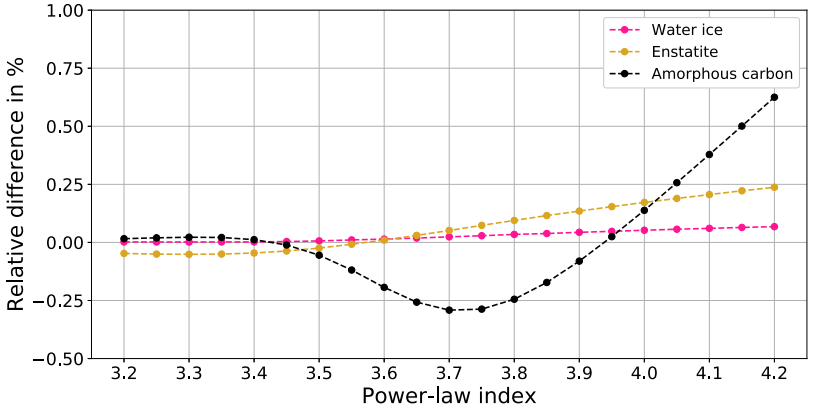

Fig. 3. Relative deviation of $Af\rho(425\,\mathrm{nm})/Af\rho(900\,\mathrm{nm})$ for the different dust compositions caused by a dust production rate day–night asymmetry compared to isotropic force-free radial outflow for ρ = 1500 km.

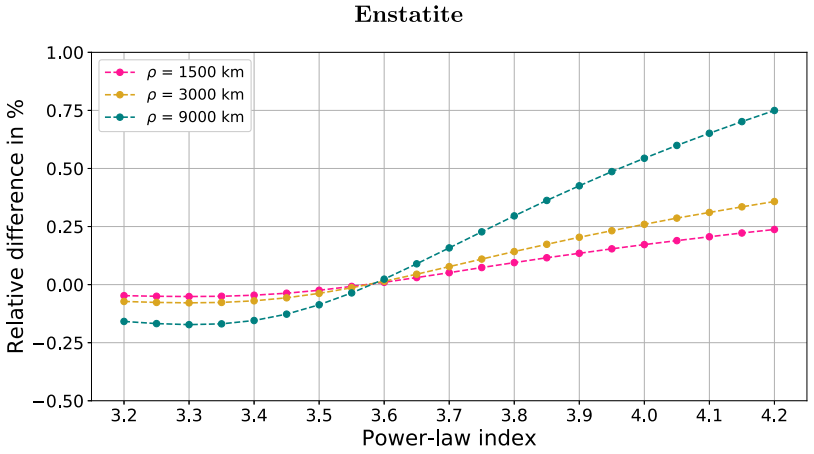

Fig. 4. Relative deviation of $Af\rho(425\,\mathrm{nm})/Af\rho(900\,\mathrm{nm})$ caused by a dust production rate day–night asymmetry compared to isotropic force-free radial outflow for ρ = 1500 km, ρ = 3000 km and ρ = 9000 km. The scattering properties are based on Enstatite.

important for the numerical model and is fulfilled by default in the case of the force-free radial outflow model.

The acceleration zone of the dust is not modelled. It is assumed that the dust particles are ejected at terminal velocity. As described in Divine et al. (1986) the dust particles move along independent ballistic trajectories outside of the acceleration zone. Such a model is valid for $R > 10R_N$, which is generally considered to be beyond the acceleration region (Gerig et al., 2018; Zakharov et al., 2021b).

The particle size distribution is modelled by using a power-law of the form $n_d(a) \propto a^{-\kappa}$, where a is the particle size and κ is the power-law index. We assume implicitly that the particle size distribution is continuous. The input to our model is the particle size distribution emitted at the nucleus surface. The particle size distribution in the coma is less steep compared to the size distribution at the surface, because larger particles get accelerated to lower velocities. The power-law index of the size distribution in the coma is approximately $\kappa_{\mathrm{coma}} \approx \kappa - 0.5$ (see

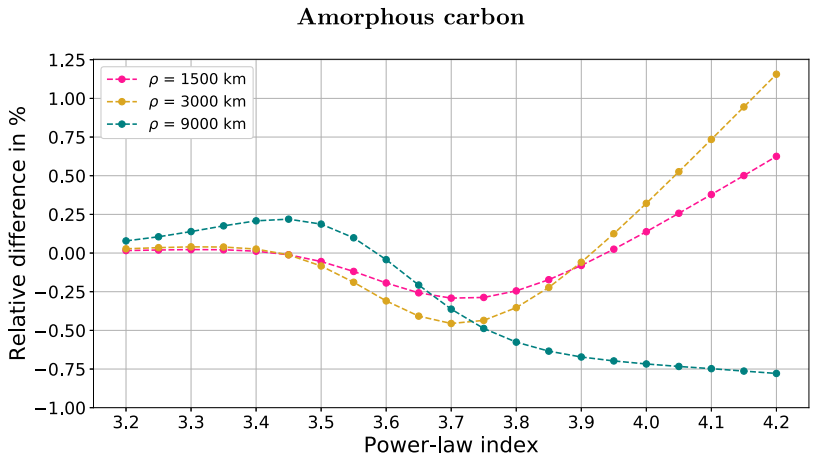

Fig. 5. Relative deviation of $Af\rho(425\,\mathrm{nm})/Af\rho(900\,\mathrm{nm})$ caused by a dust production rate day–night asymmetry compared to isotropic force-free radial outflow for ρ = 1500 km, ρ = 3000 km and ρ = 9000 km. The scattering properties are based on Amorphous carbon.

Fink and Rubin, 2012; Marschall et al., 2020; Gerig, 2021). The particle sizes are assumed to be in the range 0.01 μm to 0.1 m. The lower cut-off of the particle size distribution is chosen such that smaller particles are negligible for the calculation of $Af\rho$. As shown in Moosmüller and Sorensen (2018) the scattering efficiency drops off quickly for size parameters $\frac{2\pi a}{\lambda} < 1$. Hence, we can justify a cut-off at a_{min} = 0.01 μm, which corresponds to a size parameter of 0.15 at a wavelength of 425 nm. Additionally, the smallest particle size measured in dust measurements of McDonnell et al. (1987) and Stardust (Hörz et al., 2006) is approximately 0.01 μm. The largest considered particle size is chosen as a_{max} = 0.1 m. This choice was made based on observations of the dust by the OSIRIS instrument (Keller et al., 2007) at comet 67P/Churyumov–Gerasimenko, which found that most particles are smaller than 0.1 m (see Ott et al., 2017).

The dust particles are assumed to be spherical and homogeneous. This permits the scattering properties of the dust particles to be calculated based on Mie scattering theory as described by Kerker et al. (1983), Bohren and Huffman (1998), Mishchenko (2007). We used a code written by Moteki (2016) that we slightly modified to output the scattering properties we need (i.e. scattering efficiency, radiation pressure efficiency and phase function). We note that assuming spherical and homogeneous particles is not a realistic representation of cometary dust. That particles are not spherical was shown by in situ measurements of collected dust by MIDAS (Micro-Imaging Dust Analysis System) at comet 67P/Churyumov–Gerasimenko (Mannel et al., 2016) and by Stardust at comet 81P/Wild (Wild 2) (Kearsley et al., 2008; Brownlee, 2014). State of the art dust models use fractal aggregate dust particles or agglomerated debris particles (see Halder, 2022; Halder and Sengupta, 2023). T-matrix calculations as described by Mishchenko et al. (1996) are an intermediate approach. Even though those models can provide a more realistic representation of cometary dust the exact properties of dust aggregates and the respective composition of their sub-units is still not known. Hence, more complex dust models introduce a large number of unconstrained free parameters. With our approach the parameter space is explored without this issue. Further, at the moment the use of state of the art models is not yet a viable option for our application, because even for relatively small particles (i.e. ≈ 1 μm) high performance computing facilities are needed. Modelling such a wide range of different particles (in size and composition) as needed for this work is therefore not yet feasible. By using Mie scattering we are able to model the scattering properties for the large number of particle sizes required for this study. We chose the number of size bins by searching for convergence. For our dust model it was found that using 112 particle size bins (16 size bins per decade) is sufficient by comparing it to the results produced when using 700 particle size bins (< 1% difference). Note that if the number of particle size bins is too small, it can lead to over- or underestimations of the brightness ($Af\rho$), because there is a large variation in the brightness ($Af\rho(a)$) in relation to the particle size. The $Af\rho(a)$ is illustrated for 112 size bins for two power-law indexes in Fig. 15. By using dust compositions that are vastly different in their complex refractive index (see Table 1) we can model a wide range of scattering behaviour even if the dust particles are spherical. Further, Fink and Rubin (2012) compared rotationally symmetric ellipsoids, cylinders and Chebyshev particles as described by Mishchenko (1991) to spherical particles and found that the resulting phase functions and scattering cross sections agreed to within a few percent. They used a size parameter of 12.56 with equivalent geometric cross sections or volumes for the different particles. As shown by Pollack and Cuzzi (1980), Mie scattering can still be used for $\frac{2\pi a}{\lambda} \lesssim 20$ even if the particles are not perfectly spherical as long as the particles remain compact and have a roughly spherical shape. For size-distributions that are dominated by small particles (i.e. $\kappa \gtrsim 3.7$) the relevant particle sizes (i.e. $a \lesssim 1$ μm for λ = 425 nm and $a \lesssim 3$ μm for λ = 900 nm, also see Fig. 15) correspond to size parameters smaller than ∼ 20. Further, we compared $Af\rho$ values of our model to the values retrieved from the model by Marschall et al. (2022) which uses the scattering model described by Markkanen and Agarwal (2019). Note that when comparing the models the power-law indexes are shifted by about 0.5, because in their model it corresponds to the size distribution in the coma whereas in our model the power-law index corresponds to the size distribution at the surface. We reiterate that the difference is caused by the dispersion in dust speeds which is $v_d(a) \propto a^{-0.5}$ (see Fink and Rubin, 2012; Marschall et al., 2020; Gerig, 2021). We used a wavelength of 550 nm and found that the two models are in good agreement. In fact in the cases we tested, our model can produce the same $Af\rho$ for a wider range of dust production rates (e.g. for $Af\rho$ = 11 m with κ_{coma} = 3.6 our model predicts a dust production rate Q_d of approximately 2000 kg s^{-1} to 65000 kg s^{-1}, while their model predicts 6000 kg s^{-1} $\lesssim Q_d \lesssim$ 40000 kg s^{-1}). This is most likely due to the vastly different dust compositions used in our model. The comparison indicates that the use of Mie scattering in our model produces reliable values for $Af\rho$. Based on an analysis of the scattering behaviour of inhomogeneous particles by Gronarz et al. (2019) we estimate that the effect of inhomogeneities is smaller than 10%.

The dust particle bulk density is invariant with respect to the particle size. We validated this assumption by comparing the parameter space of using invariant dust bulk densities to a varying density model stating that $\rho_d(a) = 3.0 - 2.2(\frac{a}{a+a_0})$ with a_0 = 2 μm as described by Divine et al. (1986) (see Fig. 7).

The comet nucleus is assumed to be spherical. It was shown by Benseguane (2023) that a spherical nucleus is a good approximation in most cases.

The dust emission is assumed to be spatially and temporally homogeneous or that any inhomogeneities in the dust emission at the surface are blurred through non point source emission and lateral transport within the acceleration region ($R < 10R_N$). Kramer et al. (2018) showed that modelling the dust emission as homogeneous and static is in good agreement with observations at comet 67P/Churyumov–Gerasimenko.

The terminal outflow velocity is calculated with an identical approach to the model described in Marschall et al. (2022) and a more detailed description of the underlying assumptions can be found in Zakharov et al. (2021a) and Zakharov et al. (2021b). The equation used to describe the particle motion is valid for spherical, homogeneous and isothermal dust particles with an invariable size and mass (see Crifo et al., 2005). Further, it is assumed that the gas flow is independent of the dust (i.e. no back-coupling and no dust sublimation or re-condensation, Yamamoto and Ashihara, 1985).

2.2. Calculation of $Af\rho$

In the simplest model (isotropic force-free radial outflow), $Af\rho$ can be calculated analytically by

$$Af\rho(\lambda,\phi) = \pi \sum_a a^2 Q_{sca}(a,\lambda) p(a,\phi,\lambda) \frac{Q_d(a)}{2v_d(a)}, \tag{1}$$

where $Q_d(a)$ is the size specific dust production rate and $v_d(a)$ is the size specific outflow velocity (Fink and Rubin, 2012). In both the analytical and the numerical dust model the filling factor f can be calculated by $f = \frac{N\sigma_{geom}}{\pi\rho^2}$, where N is the total number of dust particles within an aperture of projected radius ρ and σ_{geom} is the geometric cross-section of a single particle. To calculate N a column integration is performed. By taking the sum over all size bins, $Af\rho$ is given by

$$Af\rho(\lambda,\phi) = \frac{1}{\rho} \sum_a N(a) a^2 Q_{sca}(a,\lambda) p(a,\phi,\lambda), \tag{2}$$

where $N(a)$ is the total number of dust particles of a given size seen by a aperture of projected radius ρ.

The relative contribution of each particle size bin to $Af\rho$ varies with the wavelength. This is due to the wavelength dependence of Q_{sca}. Specifically, the scattering efficiency in Mie theory is dependent on the size parameter $\frac{2\pi a}{\lambda}$ and the complex refractive index. For example using a complex refractive index of $\underline{n} = 1.5 + 0\,i$ the maximum scattering efficiency is achieved when $2a \approx \lambda$ (see Moosmuller and Ogren, 2017). Hence, we expect that the spectral ratio of $\frac{Af\rho(\lambda_1)}{Af\rho(\lambda_2)}$ for $\lambda_1 < \lambda_2$ is positively correlated with the power-law index. In this work, we calculate the spectral ratio of $\frac{Af\rho(425\,\mathrm{nm})}{Af\rho(900\,\mathrm{nm})}$ in the parameter space of our numerical model and relate it to the power-law index. The studied parameters are dust composition (as defined through the refractive index), outflow velocity and the dust production rate day–night asymmetry.

The calculated spectral ratio is based on the assumption of infinitesimal bandwidths. By testing bandwidths up to 100 nm (simulating broad-band photometry), we found that the effect of bandwidth for $\frac{Af\rho(425\,\mathrm{nm})}{Af\rho(900\,\mathrm{nm})}$ is less than 1%.

To calculate the dust number densities in the coma, test particles are emitted for all emission angles (θ, see Fig. 1). Using the listed assumptions the trajectory of each test particle can be computed analytically, because the dynamics of the dust particles are driven by the solar radiation pressure outside of the acceleration region (see Divine et al., 1986). For each grid cell the number of test particles is then scaled to calculate the dust number density.

To calculate the effects of a dust production rate day–night asymmetry we chose ρ as 1500 km, 3000 km and 9000 km. ρ needs to be chosen such that $\rho/R_N \geq 10$ to ensure that $Af\rho$ is calculated beyond the acceleration region as described by Thomas and Keller (1990) for comet 1P/Halley, Gerig et al. (2018) for comet 67P/Churyumov–Gerasimenko and Zakharov et al. (2021b) in theoretical calculations.

The dust production rate day–night asymmetry is modelled with a cosine-law of the form $Q_d(\theta) = Q_d(1 + \cos\theta)$, where θ is the emission angle. In reality, a dust production rate asymmetry would most likely be related to an asymmetry in the outflow velocity. However, for the purpose of this work it is more interesting to study an asymmetry in only the dust production rate, because it leads to a larger asymmetry in the coma. An additional asymmetry in the outflow velocity $v_d(\theta) = v_d(1 + \cos\theta)$ was tested and reduces the effects of the day–night asymmetry on the spectral ratio by approximately one order of magnitude. The reason is that a lower outflow velocity on the nightside reduces the observed day–night brightness asymmetry as is clear from the continuity equation.

Because $Af\rho$ is directly proportional to the dust production rate it cancels out when taking the spectral ratio. For this reason the spectral ratio of $Af\rho$ is independent of the dust production rate and by extension the dust-to-gas ratio.

2.3. Estimation of the outflow velocity

The outflow velocity is estimated based on an approximation of the numerical solution as described by Zakharov et al. (2021b) and Marschall et al. (2022). It is calculated by

$$v_d(a) = \frac{58.903\sqrt{T_N}}{1 + 0.6\sqrt{1.5/Iv}}, \tag{3}$$

with

$$Iv = 4.038 \cdot 10^{-29} \frac{Q_g}{R_N \rho_d a \sqrt{T_N}}, \tag{4}$$

where T_N is the surface temperature of the nucleus, Q_g is the gas production rate in molecules per second (in our case we assume pure H_2O gas with a molecular mass of 18 g/mol), R_N is the nucleus radius and ρ_d is the bulk dust density. All parameters except the gas production rate are in SI units. The maximum nucleus radius is set at 15 km, which is based on the size-frequency derived from the observation of 150 long period comets by Pan-STARRS1 (Boe et al., 2019) and the size-frequency distribution for Jupiter family comets (Belton, 2014). The range of nucleus surface temperatures is chosen to be 280-340 K and is based on the observed temperatures of comet 9P/Tempel 1 (Groussin et al., 2007) and comet 1P/Halley (Emerich et al., 1987). The bulk dust density is varied between 400 and 1600 kg m^{-3}. This range is informed by measurements of the Rosetta mission at comet 67P/Churyumov–Gerasimenko of both the average bulk density of dust particles (Fulle et al., 2016) and the density of the nucleus (Jorda et al., 2016).

2.4. Dust composition

In Table 1 the different dust compositions and their complex refractive indexes at the used wavelengths are listed. The different dust compositions were chosen to account for a wide range of complex refractive indexes. As a bright material with no absorption we chose water ice as detected by Deep Impact (Schulz et al., 2006). We chose enstatite as the silicate composition in our model (see Hanner, 1999; Ishii et al., 2008). We note that other silicate materials such as olivine are viable alternatives. However, compared to the differences in the scattering behaviour within the dust compositions used in our model, the difference between different silicates is small. As a dark carbonaceous material we chose amorphous carbon which was detected by Stardust (Matrajt et al., 2008) and is in good agreement with infrared observations (Colangeli et al., 1989; Wooden et al., 2017; Woodward et al., 2021). Carbon-rich dust particles were also detected by COSIMA onboard Rosetta (Bardyn et al., 2017).

Table 1
List of dust compositions and their complex refractive indexes for the different wavelengths used in this work. The values are taken from Hale and Querry (1973) for water ice, from Rucks et al. (2022) and Egan and Hilgeman (1975) for enstatite and from Stagg and Charalampopoulos (1993) for amorphous carbon. The complex refractive index at 550 nm was only used to calculate the radiation pressure efficiencies.

Composition	$\underline{n}$ at 425 nm	$\underline{n}$ at 550 nm	$\underline{n}$ at 900 nm
Water ice	$1.34 + 0\,i$	$1.33 + 0\,i$	$1.33 + 0\,i$
Enstatite	$1.66 + 0.00003\,i$	$1.66 + 0.00002\,i$	$1.66 + 0.00043\,i$
Amorphous carbon	$2.23 + 1.10\,i$	$2.33 + 0.99\,i$	$2.53 + 0.84\,i$

2.5. Parameter space

We explore the parameter space of our model with two approaches. In the first approach the parameters are varied independently of each other to quantify the effect of each parameter individually. We set a baseline case that keeps all the parameters constant except the parameter that is varied. Our baseline case is based on a gas production rate Q_g of 7000 kg s^{-1}, a nucleus surface temperature T_N of 310 K, a nucleus radius R_N of 4000 m, a dust bulk density ρ_d of 800 kg m^{-3} and a phase angle of 90° using the scattering properties of enstatite using the force-free radial outflow model (i.e. no day–night asymmetry). The values are independent of ρ, because the force-free radial outflow model is used. To study the day–night asymmetry the same baseline case is used, but we use the numerical model and vary both ρ and the dust composition. In the second approach all parameters except the phase angle are varied to find the most extreme cases and with it the boundaries of our parameter space. The phase angle is not varied, because for a given observation of a comet the phase angle will be well known and therefore there will be no significant uncertainty due to phase angle effects.

3. Results

In Figs. 11–14 the relation of the spectral ratio of $\frac{Af\rho(425\,\mathrm{nm})}{Af\rho(900\,\mathrm{nm})}$ to the power-law index of the particle size distribution for the whole parameter space of our model is shown. We find a correlation of the spectral ratio $\frac{Af\rho(425\,\mathrm{nm})}{Af\rho(900\,\mathrm{nm})}$ with the power-law index. Further, the effect of the particle size distribution on the spectral ratio dominates for power-laws steeper than $\kappa \approx 3.7$. In the following the individual parameters are discussed in detail.

3.1. Dust composition

In Fig. 2 we show how the spectral ratio of $\frac{Af\rho(425\,\mathrm{nm})}{Af\rho(900\,\mathrm{nm})}$ is affected by different dust compositions. The correlation of the spectral ratio of $Af\rho$ to the power-law index follows a similar trend for all modelled dust compositions. But, especially for pure water ice particles, there is a significant deviation from the other compositions for all particle size distributions. The change in the spectral ratio of $Af\rho$ due to the dust composition is comparable to the change due to the particle size distribution for power-law indexes below ~3.5.

3.2. Day–night asymmetry

As shown in Figs. 3–5, we found that the deviation of $\frac{Af\rho(425\,\mathrm{nm})}{Af\rho(900\,\mathrm{nm})}$ due to both reflected particles or day–night asymmetries compared to an isotropic force-free radial outflow model are negligible (less than 1.25%). The deviation fluctuates for different particle size distributions and dust compositions, because the radiation pressure efficiency is dependent on both particle size and scattering properties of the dust. As shown in Figs. 3 and 5 the effect of the day–night asymmetry is the largest in the case of amorphous carbon, which is explained by the larger radiation pressure efficiency. But, independent of the power-law index, the deviation is orders of magnitude smaller than the effects caused by varying dust composition or activity levels and, in practise, probably undetectable. For this reason, we use the force-free radial outflow model to study the other parameters, which optimizes the running time.

3.3. Outflow velocity

In the isotropic case of force-free radial outflow the dust number density is inversely proportional to the outflow velocity of the dust. As seen in Eqs. (3) and (4), the relationship between the particle size and the size specific outflow velocity is non-linear. This leads to a change in the observed particle size distribution in the coma outside of the acceleration zone compared to the particle size distribution emitted at the surface of the nucleus (see also McDonnell et al., 1987). We remind the reader again that the power-law index at the surface (which is the input to our model) and the power-law index in the coma are linked by $\kappa_{\mathrm{coma}} \approx \kappa - 0.5$. The dust production rate Q_d, the nucleus radius r_N and the nucleus surface temperature T_N cannot be assumed to be independent of each other. Therefore, instead of varying each of those three parameters individually it is more appropriate to study them together in what we call a low, medium and high activity case as shown in Fig. 6.

Another parameter affecting the outflow velocity is the dust bulk density. In Fig. 7, low (ρ_d = 400 kg m^{-3}), intermediate (ρ_d = 800 kg m^{-3}) and high (ρ_d = 1600 kg m^{-3}) dust bulk density cases are shown. In addition, the constant dust bulk densities are compared to a density model as described by Divine et al. (1986). The density model accounts for smaller particles being more compact and hence having larger densities. However, in Fig. 7 it is shown that the density model is included in the parameter space of the constant dust bulk densities. As expected, the results of the density model are closer to a low dust bulk density for large particle dominated size distributions and closer to a high dust bulk density for small particle dominated size distributions.

Both the activity and the bulk dust density influence the spectral ratio more significantly for steeper power-law size distributions, as seen in Figs. 6 and 7. The changes in the spectral ratio as a result of different outflow velocities are due to a change in the particle size distribution in the coma compared to the particle size distribution at the nucleus surface. Hence, the results shown in Figs. 6 and 7 give an indication of how precise the relationship $\kappa_{\mathrm{coma}} \approx \kappa - 0.5$ is.

3.4. Phase angle

In Figs. 8–10 the spectral ratio of $Af\rho$ is shown for varying phase angles for different dust compositions. We find that there is a similar correlation between the spectral ratio of $Af\rho$ and the power-law index for all phase angles. The strength of the phase angle effects is strongly dependent on the dust composition. The spectral ratio in the case of amorphous carbon particles is the least affected by varying phase angles as shown in Fig. 10. For water ice particles, as shown in Fig. 8, the spectral ratio of $Af\rho$ varies by up to ~25%. The largest phase angle effects occur for enstatite particles that show large phase angle effects (up to ~40% difference) for power-law indexes smaller than 3.7 as shown in Fig. 9.

3.5. Constraints on the particle size distribution

The tightness of the constraints that can be placed on the power-law index depends on the phase angle (see Figs. 11–14). In the best case (see Fig. 11) the power-law index can be constrained to an uncertainty of ±0.1 for small particle dominated comae, whereas in the worst case (see Fig. 12) the uncertainty is about ±0.2. The lower boundary is found for the inputs Q_g = 1000 kg s^{-1}, R_N = 1000 m, T_N = 280 K and ρ_D = 1600 kg m^{-3}. The upper boundary is found for the inputs Q_g = 40,000 kg s^{-1}, R_N = 15,000 m, T_N = 340 K and ρ_D = 400 kg m^{-3}. Note again that the results are dependent on Q_g, R_N and T_N through

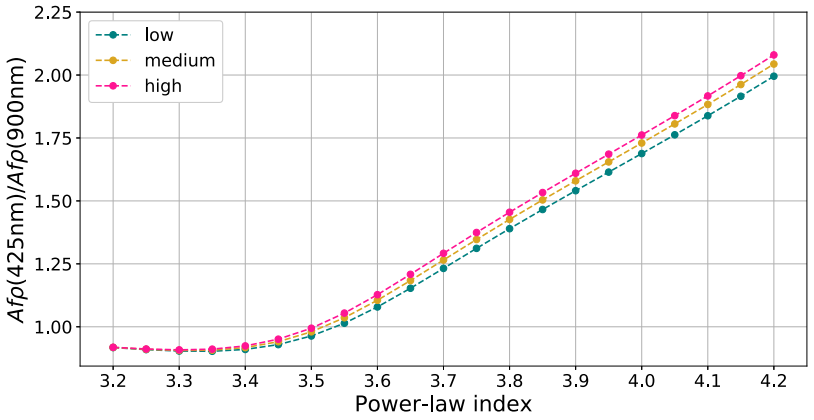

Fig. 6. Spectral ratio of $Af\rho$ in relation to the power-law index for three different activity levels. The corresponding input parameters are Q_g = 1000 kg s^{-1}, R_N = 1000 m and T_N = 280 K for low activity, Q_g = 7000 kg s^{-1}, R_N = 4000 m and T_N = 310 K for medium activity and Q_g = 40,000 kg s^{-1}, R_N = 15,000 m and T_N = 340 K for high activity. The bulk dust density is not varied and set as ρ_d = 600 kg m^{-3}.

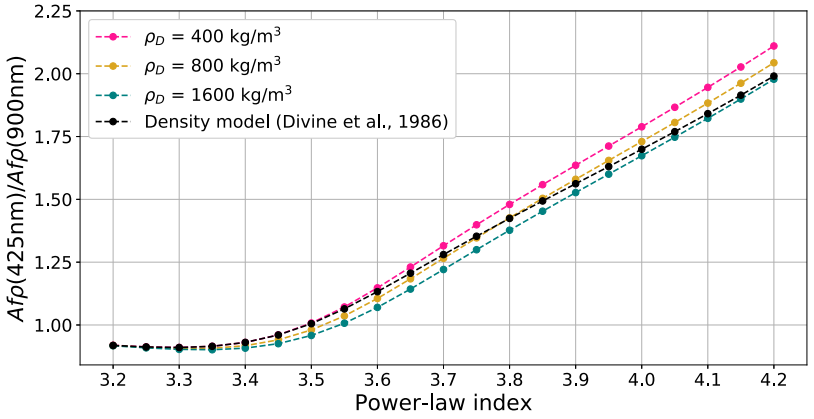

Fig. 7. Spectral ratio of $Af\rho$ in relation to the power-law index for varying dust bulk densities. The remaining parameters are set at Q_g = 7000 kg s^{-1}, R_N = 4000 m and T_N = 310 K. The scattering properties are based on astronomical silicate.

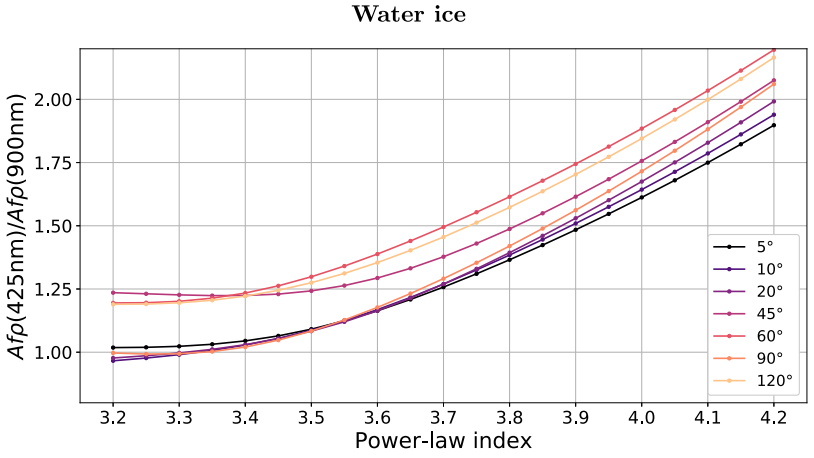

Fig. 8. Spectral ratio of $Af\rho$ in relation to the power-law index for varying phase angles between 5° to 120° in the case of a water ice dust composition.

the calculation of the terminal dust velocity. The dust composition corresponding to the boundaries depends on the power-law index and phase angle (also see Figs. 2 and 11–14). Because of the lack of information on the statistical distribution of the input parameters to our model, probability intervals cannot be provided. To allow for rough estimations of the particle size distributions we fitted a function of the form $\kappa = a + b\sqrt{x + c}$, where x is the spectral ratio of $Af\rho$ to the mean values taken over all the boundaries of the different compositions. We recommend that the fits are only used for $\frac{Af\rho(425\,\mathrm{nm})}{Af\rho(900\,\mathrm{nm})} \gtrsim 1.25$, because the uncertainty is too large otherwise. We also note that the fits are undefined for $\frac{Af\rho(425\,\mathrm{nm})}{Af\rho(900\,\mathrm{nm})} + c < 0$.

4. Discussion

As shown in Figs. 11–14 a spectral ratio of $Af\rho$ can be used to constrain the power-law index of the particle size distribution. The

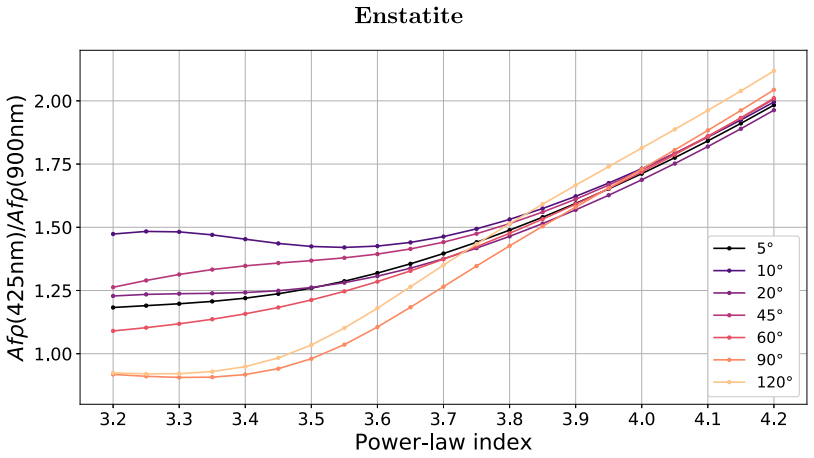

Fig. 9. Spectral ratio of $Af\rho$ in relation to the power-law index for varying phase angles between 5° to 120° in the case of an enstatite dust composition.

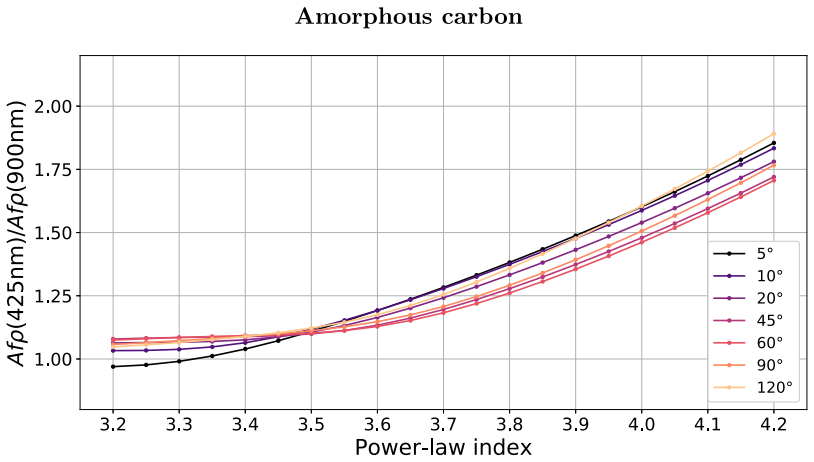

Fig. 10. Spectral ratio of $Af\rho$ in relation to the power-law index for varying phase angles between 5° to 120° in the case of an amorphous carbon dust composition.

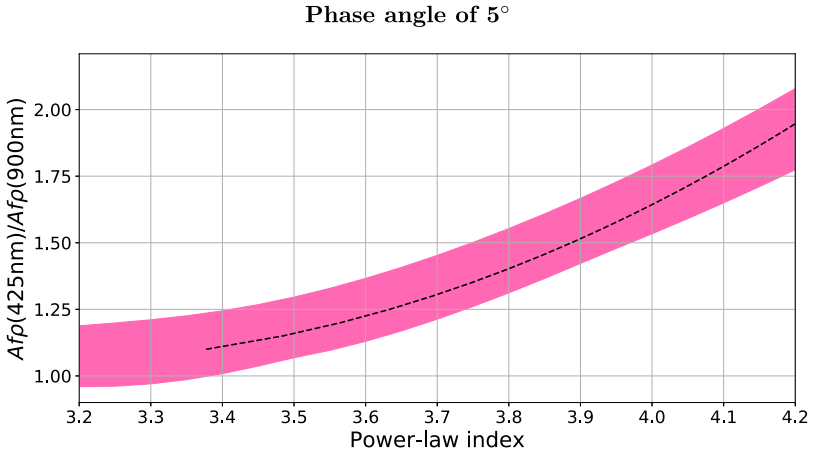

Fig. 11. Total model range of $Af\rho$(425 nm)/$Af\rho$(900 nm) for a phase angle of 5° in relation to the power-law index corresponding to the modelled parameter space. It shows the total uncertainties due to the variation of the dust composition (see Table 1 and Fig. 2), activity from Q_g = 1000 kg s^{-1}, R_N = 1000 m and T_N = 280 K to Q_g = 40,000 kg s^{-1}, R_N = 15,000 m and T_N = 340 K (see Fig. 6) and dust bulk density from 400 kg m^{-3} to 1600 kg m^{-3} (see Fig. 7). The black line is a fit to the mean values ($\kappa \approx 3.13 + 1.23\sqrt{x - 1.05}$, with x being the spectral ratio of $Af\rho$).

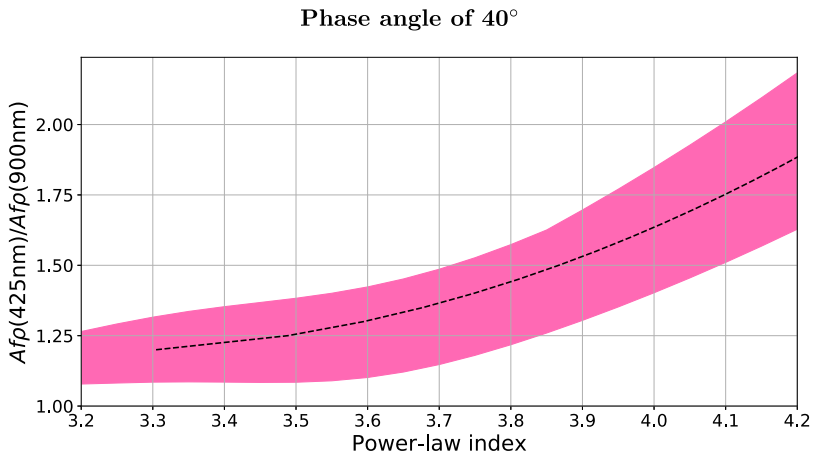

Fig. 12. Total model range of the spectral ratio of $Af\rho$ in relation to the power-law index for a phase angle of 40°. The fit to the mean values (black line) is $\kappa \approx 3.20+1.20\sqrt{x-1.19}$, with x being the spectral ratio of $Af\rho$.

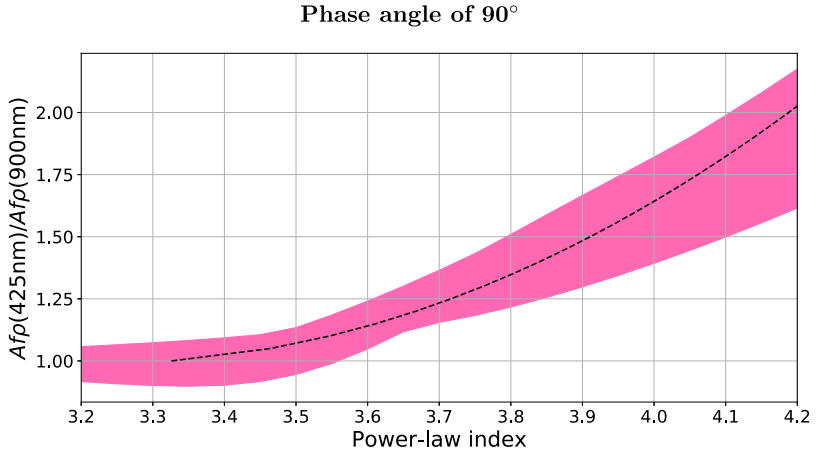

Fig. 13. Total model range of the spectral ratio of $Af\rho$ in relation to the power-law index for a phase angle of 90°. The fit to the mean values (black line) is $\kappa \approx 3.23+0.95\sqrt{x-0.99}$, with x being the spectral ratio of $Af\rho$.

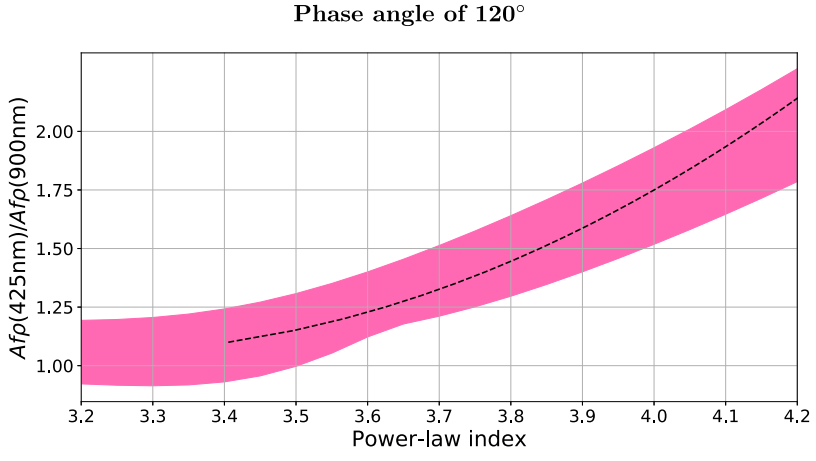

Fig. 14. Total model range of the spectral ratio of $Af\rho$ in relation to the power-law index for a phase angle of 120°. The fit to the mean values (black line) is $\kappa \approx 3.20+0.95\sqrt{x-1.05}$, with x being the spectral ratio of $Af\rho$.

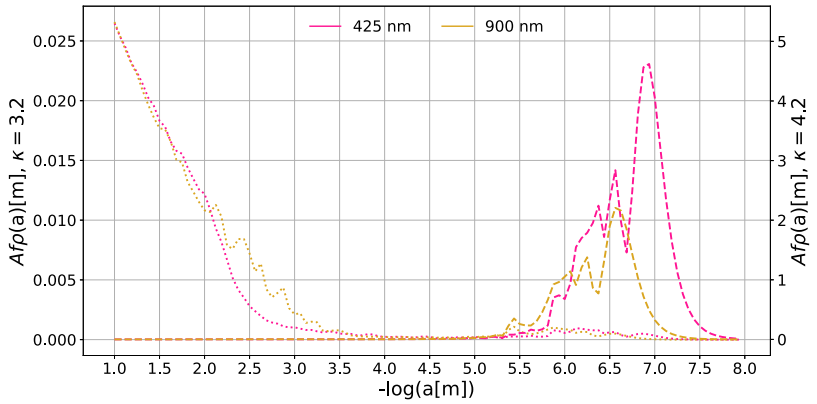

Fig. 15. The plot shows $Af\rho(a,\lambda)$ for both 425 nm (pink) and 900 nm (yellow) using enstatite dust particles following a size distribution with a power-law index of $\kappa = 3.2$ (dotted) and $\kappa = 4.2$ (dashed). The baseline case as described in the methods section is used with a dust production rate of $Q_d = 3500\text{kg s}^{-1}$. For a power-law index of $\kappa = 3.2$ the total $Af\rho(\lambda)$ (which is the sum over all particle size bins) is 0.41 m for 425 nm and 0.45 m for 900 nm, whereas for a power-law index of $\kappa = 4.2$ the total $Af\rho(\lambda)$ is 54.1 m for 425 nm and 26.5 m for 900 nm.

main limitation of this method is the implicit assumption that the particle size distribution follows a power-law. In most cases the dust size distribution does not follow a simple power-law, as measured at comet 1P/Halley (McDonnell et al., 1987) and at comet 67P/Churyumov–Gerasimenko (Merouane et al., 2016; Rinaldi et al., 2017). In both cases the size distribution was fitted by a more complicated power-law distribution with changes in the power-law index at certain particle sizes. However, our modelling predicts that the wavelength dependence in large particle dominated size distributions is small in comparison to the wavelength dependence in small particle dominated size distributions. A distinction between small particle dominated and large particle dominated dust size distributions should therefore be possible nevertheless. The contribution of each particle size bin to $Af\rho$ is illustrated for a small particle dominated and a large particle dominated size distribution in Fig. 15. If light scattering is dominated by large particles the wavelength dependence of $Af\rho$ is mostly lost. The loss of the wavelength dependence can also be seen in Figs. 11–14, where $\frac{Af\rho(425\,\text{nm})}{Af\rho(900\,\text{nm})} \approx 1$ for $\kappa = 3.2$. For this reason, in a large particle dominated regime the power-law index is least constrained by the $Af\rho$ ratio. For steep particle size distributions with power-law indexes above ~ 3.7 the light scattering is strongly dominated by particles smaller than ~ 3 μm at a wavelength of 900 nm and smaller than ~ 1 μm at a wavelength of 425 nm. Further, in Fig. 15 it is illustrated that even with a steep power-law index of $\kappa = 4.2$ most of the light is scattered by particles larger than 0.1 μm. Hence, in small particle dominated size distributions the constraints on the power-law index are valid for a size range of approximately 0.1 μm - 4 μm, because it is the particle sizes in that range that scatter the light.

An additional uncertainty arises from the assumption of spherical and homogeneous particles. The justification for this assumption is extensively discussed in the methods section. The results of this work clearly show that the particle size distribution has a dominant effect over all other parameters even if the scattering properties of the dust composition are varied significantly. However, if state of the art models get computationally more manageable or if the relevant scattering properties are being provided our model could be easily adapted to different scattering models. A more precise modelling of the scattering behaviour of the dust could reduce the uncertainty of the model and further improve the constraints on the power-law index. We note that in the context of the method described in this work more sophisticated dust model still need to account for a range of dust compositions, because cometary dust might be compositionally diverse (see Wooden et al., 2017). For more complex dust particles such as fractal aggregates dust particles or agglomerated debris particles as described by Halder (2022), Halder and Sengupta (2023) it might be necessary to modify the equations used to calculate the outflow velocities (see Eq. (3) and (4)) to keep the model self consistent. We remind the reader again that the dust dynamics calculations assume spherical and homogeneous particles as well (see Crifo et al., 2005; Zakharov et al., 2021a,b; Marschall et al., 2022). Assuming a constant dust particle density for all the dust particle sizes, overestimates the influence of larger particles on $Af\rho$, because the outflow velocity of those particles is underestimated. But, we show in Fig. 7 that using a density model as described by Divine et al. (1986) lies within the parameter space of the constant dust bulk densities used in our modelling. To make the most reliable constraints on the power-law index it is recommended to use $\rho < 270\,R_N$ (which corresponds to $\rho < 1500$ km in the case of comet 1P/Halley), because beyond that region a large percentage of the deviations of the column density to ρ^{-1} is most likely due to gas contributions if broad-band photometry is used (see Thomas and Keller, 1990). If a standard aperture radius of $\rho = 10000$ km (see Opitom et al., 2017; Betzler et al., 2023) is used, possible gas contributions need to be evaluated more carefully. We note that for signal to noise reasons, the use of broad-band photometry is likely to be most frequent. If the gas contribution is significantly large it can introduce a wavelength dependency of $Af\rho$ that is not considered in our model. It is further advised that broad-band filters are only used if the gas emission lines are expected to be weak. To avoid significant gas emission lines, narrow-band filters might be preferable in some cases. Otherwise corrections of the spectral ratio of $Af\rho$ might be necessary. In most cases, the measured photometric colour of cometary dust is red (i.e. $\frac{Af\rho(425\,\text{nm})}{Af\rho(900\,\text{nm})} < 1$, see Jewitt and Meech, 1986). Based on the modelling of this work, a red colour indicates a coma that is dominated by large particles and that there is no significant water ice component. Alternatively, the red colour can potentially be explained by size distributions different from a simple power-law, where the smallest particles are not the most abundant. Variations in the spectral ratio for different aperture sizes indicate either a change in the dust composition or a change in the size distribution which could indicate a fragmentation of the dust (see Combi, 1994; Jones et al., 2008). For comet 2P/Encke it was found by Jewitt (2004) that the colour of the dust gets bluer with increasing distance from the nucleus. This effect was explained by suggesting that there are more small particles further away due to fragmentation. A similar result was found for comet 67P/Churyumov–Gerasimenko by Rosenbush et al. (2017). Our work supports the hypothesis that the blueward shift is most likely caused by a change in the dust size distribution.

5. Conclusion

We show how spectral ratioing of $Af\rho$ can be used to constrain the power-law index of the particle-size distribution. In a small particle dominated regime ($\kappa \gtrsim 3.7$) the power-law index can be constrained

to an uncertainty of about ±0.1 to ±0.2 depending on the phase angle. Further, the constraints on the power-law index for an observed comet could be improved by better constraining some of the inputs to our model (i.e. nucleus surface temperature, nucleus radius or gas production rate). The results of this work further strengthen the hypothesis that dust environments with a larger number of smaller particles are more blue as discussed by Cochran et al. (2015). The modelling can be done for any two wavelengths, but clearly the wider the separation, the stronger the effects assuming that the wavelengths are dominated by scattered light as opposed to thermal emission. If standard photometric filters are used, we recommend using the B and I filters in the UBVRI system or g' and z' in the SDSS system (see Bessell, 2005). The blue and red HB filters as described by Farnham et al. (2000) would be another option. Filter pairs with a narrower separation can be used, but will result in looser constraints on the particle size distribution. Further, the constraints on the power-law index from this method can be used to make conversions from the brightness ($A f \rho$) to the dust production rate more precise as discussed by Marschall et al. (2022). We find similar trends to those described in the work by Voitko et al. (2022, 2024). To conclusively explain the red colour seen in most observations, more sophisticated particle size distributions need to be modelled and studied. For future cometary fly-by missions simultaneous measurements in the scattered visible and near-infrared would be highly beneficial in assessing the danger from dust particle impacts. Observations of comets in relation to their heliocentric distance could be used to detect changes in the particle size distributions.

CRediT authorship contribution statement

Nico Haslebacher: Writing – original draft, Visualization, Validation, Methodology, Conceptualization. **Nicolas Thomas:** Writing – review & editing, Supervision, Funding acquisition. **Raphael Marschall:** Writing – review & editing.

Declaration of competing interest

The authors declare that they have no known competing financial interests or personal relationships that could have appeared to influence the work reported in this paper.

Data availability

Data will be made available on request.

Acknowledgements

This work has been carried out within the framework of the National Centre of Competence in Research PlanetS supported by the Swiss National Science Foundation under grants 51NF40_182901 and 51NF40_205606. The development of the Coma Model for Comet Interceptor has been funded by the European Space Agency through Contract 4000136014/21/NL/CRS.

References

A'Hearn, M.F., Belton, M.J.S., Collins, S.M., Farnham, T.L., Feaga, L.M., Groussin, O., Lisse, C.M., Meech, K.J., Schultz, P.H., Sunshine, J.M., 2008. Deep impact and sample return. Earth, Planets Space (ISSN: 1880-5981) 60 (1), 61–66. http://dx.doi.org/10.1186/BF03352762.

A'Hearn, M.F., Schleicher, D.G., Millis, R.L., Feldman, P.D., Thompson, D.T., 1984. Comet bowell 1980b. Astron. J. 89, 579–591. http://dx.doi.org/10.1086/113552.

Bardyn, A., Baklouti, D., Cottin, H., Fray, N., Briois, C., Paquette, J., Stenzel, O., Engrand, C., Fischer, H., Hornung, K., Isnard, R., Langevin, Y., Lehto, H., Le Roy, L., Ligier, N., Merouane, S., Modica, P., Orthous-Daunay, F.-R., Rynö, J., Schulz, R., Silén, J., Thirkell, L., Varmuza, K., Zaprudin, B., Kissel, J., Hilchenbach, M., 2017. Carbon-rich dust in comet 67P/Churyumov-Gerasimenko measured by COSIMA/Rosetta. Mon. Not. R. Astron. Soc. (ISSN: 0035-8711) 469 (suppl2), S712–S722. http://dx.doi.org/10.1093/mnras/stx2640.

Baum, W.A., Kreidl, T.J., Schleicher, D.G., 1992. Cometary grains. Astron. J. 104, 1216. http://dx.doi.org/10.1086/116310.

Belton, M.J.S., 2014. The size-distribution of scattered disk TNOs from that of JFCs between 0.2 and 15km effective radius. Icarus (ISSN: 0019-1035) 231, 168–182. http://dx.doi.org/10.1016/j.icarus.2013.12.001, URL https://www.sciencedirect.com/science/article/pii/S0019103513005101.

Benseguane, S., 2023. From Local Topography to Global Morphology: Origins and Consequences on the Activity of Comet Nuclei (Ph.D. thesis). Université Claude Bernard Lyon 1.

Bernardinelli, P.H., Bernstein, G.M., Montet, B.T., Weryk, R., Wainscoat, R., Aguena, M., Allam, S., Andrade-Oliveira, F., Annis, J., Avila, S., Bertin, E., Brooks, D., Burke, D.L., Rosell, A.C., Kind, M.C., Carretero, J., Cawthon, R., Conselice, C., Costanzi, M., da Costa, L.N., Pereira, M.E.S., Vicente, J.D., Diehl, H.T., Everett, S., Ferrero, I., Flaugher, B., Frieman, J., García-Bellido, J., Gaztanaga, E., Gerdes, D.W., Gruen, D., Gruendl, R.A., Gschwend, J., Gutierrez, G., Hinton, S.R., Hollowood, D.L., Honscheid, K., James, D.J., Kuehn, K., Kuropatkin, N., Lahav, O., Maia, M.A.G., Marshall, J.L., Menanteau, F., Miquel, R., Morgan, R., Ogando, R.L.C., Paz-Chinchón, F., Pieres, A., Malagón, A.A.P., Rodriguez-Monroy, M., Romer, A.K., Roodman, A., Sanchez, E., Schubnell, M., Serrano, S., Sevilla-Noarbe, I., Smith, M., Soares-Santos, M., Suchyta, E., Swanson, M.E.C., Tarle, G., To, C., Troxel, M.A., Varga, T.N., Walker, A.R., Zhang, Y., (The DES Collaboration), 2021. C/2014 UN271 (Bernardinelli-Bernstein): The nearly spherical cow of comets. Astrophys. J. Lett. 921 (2), L37. http://dx.doi.org/10.3847/2041-8213/ac32d3.

Bessell, M.S., 2005. Standard photometric systems. Annu. Rev. Astron. Astrophys. 43 (1), 293–336. http://dx.doi.org/10.1146/annurev.astro.41.082801.100251.

Betzler, A.S., Diepvens, A., de Sousa, O.F., 2023. The activity of 119 comets. Mon. Not. R. Astron. Soc. (ISSN: 0035-8711) 526 (1), 246–262. http://dx.doi.org/10.1093/mnras/stad2696.

Bockelée-Morvan, D., Crovisier, J., Mumma, M.J., Weaver, H.A., 2004. The composition of cometary volatiles. In: Festou, M.C., Keller, H.U., Weaver, H.A. (Eds.), Comets II. p. 391.

Bockelée-Morvan, D., Rinaldi, G., Erard, S., Leyrat, C., Capaccioni, F., Drossart, P., Filacchione, G., Migliorini, A., Quirico, E., Mottola, S., Tozzi, G., Arnold, G., Biver, N., Combes, M., Crovisier, J., Longobardo, A., Blecka, M., Capria, M.-T., 2017. Comet 67P outbursts and quiescent coma at 1.3 au from the sun: dust properties from Rosetta/VIRTIS-H observations. Mon. Not. R. Astron. Soc. (ISSN: 0035-8711) 469 (suppl2), S443–S458. http://dx.doi.org/10.1093/mnras/stx1950.

Boe, B., Jedicke, R., Meech, K.J., Wiegert, P., Weryk, R.J., Chambers, K.C., Denneau, L., Kaiser, N., Kudritzki, R.-P., Magnier, E.A., Wainscoat, R.J., Waters, C., 2019. The orbit and size-frequency distribution of long period comets observed by Pan-STARRS1. Icarus (ISSN: 0019-1035) 333, 252–272. http://dx.doi.org/10.1016/j.icarus.2019.05.034, URL https://www.sciencedirect.com/science/article/pii/S0019103518306080.

Bohren, C., Huffman, D., 1998. Absorption and scattering by a sphere. In: Absorption and Scattering of Light By Small Particles. John Wiley & Sons, Ltd, ISBN: 9783527618156, pp. 82–129. http://dx.doi.org/10.1002/9783527618156.ch4, URL https://onlinelibrary.wiley.com/doi/abs/10.1002/9783527618156.ch4.

Brownlee, D., 2014. The stardust mission: Analyzing samples from the edge of the solar system. Annu. Rev. Earth Planet. Sci. 42 (1), 179–205. http://dx.doi.org/10.1146/annurev-earth-050212-124203.

Cambianica, P., Cremonese, G., Munaretto, G., Capria, M.T., Fulle, M., Boschin, W., Di Fabrizio, L., Harutyunyan, A., 2021. A high-spectral-resolution catalog of emission lines in the visible spectrum of comet C/2020 F3 (NEOWISE). Astron. Astrophys. 656, A160. http://dx.doi.org/10.1051/0004-6361/202140309.

Cochran, A.L., Levasseur-Regourd, A.-C., Cordiner, M., Hadamcik, E., Lasue, J., Gicquel, A., Schleicher, D.G., Charnley, S.B., Mumma, M.J., Paganini, L., Bockelée-Morvan, D., Biver, N., Kuan, Y.-J., 2015. The composition of comets. Space Sci. Rev. (ISSN: 1572-9672) 197 (1), 9–46. http://dx.doi.org/10.1007/s11214-015-0183-6.

Colangeli, L., Schwehm, G., Bussoletti, E., Blanco, A., Borghesi, A., Fonti, S., Orofino, V., 1989. Experimental evidence for amorphous carbon grains in comets. In: Allamandola, L.J., Tielens, A.G.G.M. (Eds.), In: Interstellar Dust, vol. 135, pp. 437–442.

Combi, M.R., 1994. The fragmentation of dust in the innermost comae of comets: Possible evidence from ground-based images. Astron. J. 108, 304. http://dx.doi.org/10.1086/117070.

Crifo, J.-F., Loukianov, G.A., Rodionov, A.V., Zakharov, V.V., 2005. Direct Monte Carlo and multifluid modeling of the circumnuclear dust coma: Spherical grain dynamics revisited. Icarus (ISSN: 0019-1035) 176 (1), 192–219. http://dx.doi.org/10.1016/j.icarus.2005.01.003, URL https://www.sciencedirect.com/science/article/pii/S0019103505000060.

Curdt, W., Keller, H.U., 1990. Large dust particles along the giotto trajectory. Icarus (ISSN: 0019-1035) 86 (1), 305–313. http://dx.doi.org/10.1016/0019-1035(90)90220-4, URL http://www.sciencedirect.com/science/article/pii/0019103590902204.

Divine, N., Fechtig, H., Gombosi, T.I., Hanner, M.S., Keller, H.U., Larson, S.M., Mendis, D.A., Newburn, R.L., Reinhard, R., Sekanina, Z., Yeomans, D.K., 1986. The comet halley dust and gas environment. SSR 43, 1. http://dx.doi.org/10.1007/BF00175326.

Egan, W.G., Hilgeman, T., 1975. Interstellar medium: UV complex index of refraction of several candidate materials. Astron. J. 80 (8), 587–594. http://dx.doi.org/10.1086/111782, URL https://www.osti.gov/biblio/4156980.

Emerich, C., Lamarre, J.M., Moroz, V.I., Combes, M., Sanko, N.F., Nikolsky, Y.V., Rocard, F., Gispert, R., Coron, N., Bibring, J.P., Encrenaz, T., Crovisier, J., 1987. Temperature and size of the nucleus of comet p/ halley deduced from IKS infrared VEGA-1 measurements. Astron. Astrophys. 187, 839.

Farnham, T.L., Schleicher, D.G., A'Hearn, M.F., 2000. The HB narrowband comet filters: Standard stars and calibrations. Icarus 147 (1), 180–204. http://dx.doi.org/10.1006/icar.2000.6420.

Fink, U., Rubin, M., 2012. The calculation of $Af\rho$ and mass loss rate for comets. Icarus (ISSN: 0019-1035) 221 (2), 721–734. http://dx.doi.org/10.1016/j.icarus.2012.09.001, URL https://www.sciencedirect.com/science/article/pii/S0019103512003612.

Fulle, M., Della Corte, V., Rotundi, A., Rietmeijer, F.J.M., Green, S.F., Weissman, P., Accolla, M., Colangeli, L., Ferrari, M., Ivanovski, S., Lopez-Moreno, J.J., Epifani, E.M., Morales, R., Ortiz, J.L., Palomba, E., Palumbo, P., Rodriguez, J., Sordini, R., Zakharov, V., 2016. Comet 67P/Churyumov–Gerasimenko preserved the pebbles that formed planetesimals. Mon. Not. R. Astron. Soc. (ISSN: 0035-8711) 462 (Suppl1), S132–S137. http://dx.doi.org/10.1093/mnras/stw2299.

Garcia, R., Gil-Hutton, R., García-Migani, E., 2020. Observational results for five short-period and five long-period comets. Planet. Space Sci. (ISSN: 0032-0633) 180, 104779. http://dx.doi.org/10.1016/j.pss.2019.104779, URL https://www.sciencedirect.com/science/article/pii/S0032063319302892.

Gerig, S.-B., 2021. Dust in the Inner Coma of Comet 67P/Churyumov-Gerasimenko (Ph.D. thesis). Universität Bern.

Gerig, S.-B., Marschall, R., Thomas, N., Bertini, I., Bodewits, D., Davidsson, B., Fulle, M., Ip, W.-H., Keller, H.U., Küppers, M., Preusker, F., Scholten, F., Su, C.C., Toth, I., Tubiana, C., Wu, J.S., Sierks, H., Barbieri, C., Lamy, P.L., Rodrigo, R., Koschny, D., Rickman, H., Agarwal, J., Barucci, M.A., Bertaux, J.-L., Cremonese, G., Da Deppo, V., Debei, S., De Cecco, M., Deller, J., Fornasier, S., Groussin, O., Gutierrez, P.J., Güttler, C., Hviid, S.F., Jorda, L., Knollenberg, J., Kramm, J.-R., Kührt, E., Lara, L.M., Lazzarin, M., Lopez Moreno, J.J., Marzari, F., Mottola, S., Naletto, G., Oklay, N., Vincent, J.B., 2018. On deviations from free-radial outflow in the inner coma of comet 67P/Churyumov-Gerasimenko. Icarus 311, 1–22. http://dx.doi.org/10.1016/j.icarus.2018.03.010.

Gronarz, T., Höges, C., Kez, V., Habermehl, M., Kneer, R., 2019. Comparison of scattering behaviour for inhomogeneous particles in pulverized coal combustion. Int. J. Therm. Sci. (ISSN: 1290-0729) 140, 1–7. http://dx.doi.org/10.1016/j.ijthermalsci.2019.02.034, URL https://www.sciencedirect.com/science/article/pii/S1290072918317708.

Groussin, O., A'Hearn, M.F., Li, J.-Y., Thomas, P.C., Sunshine, J.M., Lisse, C.M., Meech, K.J., Farnham, T.L., Feaga, L.M., Delamere, W.A., 2007. Surface temperature of the nucleus of comet 9P/Tempel 1. Icarus (ISSN: 0019-1035) 187 (1), 16–25. http://dx.doi.org/10.1016/j.icarus.2006.08.030, URL https://www.sciencedirect.com/science/article/pii/S0019103506003952, Deep Impact Mission to Comet 9P/Tempel 1, Part 1.

Halder, P., 2022. REST: A java package for crafting realistic cosmic dust particles. Astrophys. J. Suppl. Ser. 263 (1), 3. http://dx.doi.org/10.3847/1538-4365/ac9183.

Halder, P., Sengupta, S., 2023. A comprehensive model of morphologically realistic cosmic dust particles: An application to mimic the unusual polarization properties of the interstellar comet 2I/borisov. Astrophys. J. 947 (1), 1. http://dx.doi.org/10.3847/1538-4357/acbf52.

Hale, G.M., Querry, M.R., 1973. Optical constants of water in the 200-nm to 200-μm wavelength region. Appl. Opt. 12 (3), 555–563. http://dx.doi.org/10.1364/AO.12.000555, URL https://opg.optica.org/ao/abstract.cfm?URI=ao-12-3-555.

Hanner, M.S., 1999. The silicate material in comets. Space Sci. Rev. 90, 99–108. http://dx.doi.org/10.1023/A:1005285711945.

Haslebacher, N., Gerig, S.-B., Thomas, N., Marschall, R., Zakharov, V., Tubiana, C., 2022. A numerical model of dust particle impacts during a cometary encounter with application to ESA's comet interceptor mission. Acta Astronaut. (ISSN: 0094-5765) 195, 243–250. http://dx.doi.org/10.1016/j.actaastro.2022.02.023, URL https://www.sciencedirect.com/science/article/pii/S009457652200087X.

Hörz, F., Bastien, R., Borg, J., Bradley, J.P., Bridges, J.C., Brownlee, D.E., Burchell, M.J., Chi, M., Cintala, M.J., Dai, Z.R., Djouadi, Z., Dominguez, G., Economou, T.E., Fairey, S.A.J., Floss, C., Franchi, I.A., Graham, G.A., Green, S.F., Heck, P., Hoppe, P., Huth, J., Ishii, H., Kearsley, A.T., Kissel, J., Leitner, J., Leroux, H., Marhas, K., Messenger, K., Schwandt, C.S., See, T.H., Snead, C., Stadermann, F.J., Stephan, T., Stroud, R., Teslich, N., Trigo-Rodríguez, J.M., Tuzzolino, A.J., Troadec, D., Tsou, P., Warren, J., Westphal, A., Wozniakiewicz, P., Wright, I., Zinner, E., 2006. Impact features on stardust: Implications for comet 81P/wild 2 dust. Science 314 (5806), 1716–1719. http://dx.doi.org/10.1126/science.1135705, URL https://www.science.org/doi/abs/10.1126/science.1135705.

Ishii, H., Bradley, J., Dai, Z., Chi, M., Kearsley, A., Burchell, M., Browning, N., Molster, F., 2008. Comparison of comet 81P/wild 2 dust with interplanetary dust from comets. Science 319, 447–450. http://dx.doi.org/10.1126/science.1150683.

Jewitt, D., 2004. Looking through the HIPPO: Nucleus and dust in comet 2P/encke. Astron. J. 128 (6), 3061. http://dx.doi.org/10.1086/425888.

Jewitt, D., Meech, K.J., 1986. Cometary grain scattering versus wavelength, or, "what color is comet dust?". Astrophys. J. 310, 937. http://dx.doi.org/10.1086/164745.

Jewitt, D., Meech, K.J., 1987. Surface brightness profiles of 10 comets. Astrophys. J. 317, 992. http://dx.doi.org/10.1086/165347.

Jones, G.H., Snodgrass, C., Tubiana, C., Küppers, M., Kawakita, H., Lara, L.M., Agarwal, J., André, N., Attree, N., Auster, U., Bagnulo, S., Bannister, M., Beth, A., Bowles, N., Coates, A., Colangeli, L., Corral van Damme, C., Da Deppo, V., De Keyser, J., Della Corte, V., Edberg, N., El-Maarry, M.R., Faggi, S., Fulle, M., Funase, R., Galand, M., Goetz, C., Groussin, O., Guilbert-Lepoutre, A., Henri, P., Kasahara, S., Kereszturi, A., Kidger, M., Knight, M., Kokotanekova, R., Kolmasova, I., Kossacki, K., Kührt, E., Kwon, Y., La Forgia, F., Levasseur-Regourd, A.-C., Lippi, M., Longobardo, A., Marschall, R., Morawski, M., Muñoz, O., Näsilä, A., Nilsson, H., Opitom, C., Pajusalu, M., Pommerol, A., Prech, L., Rando, N., Ratti, F., Rothkaehl, H., Rotundi, A., Rubin, M., Sakatani, N., Sánchez, J.P., Simon Wedlund, C., Stankov, A., Thomas, N., Toth, I., Villanueva, G., Vincent, J.-B., Volwerk, M., Wurz, P., Wielders, A., Yoshioka, K., Aleksiejuk, K., Alvarez, F., Amoros, C., Aslam, S., Atamaniuk, B., Baran, J., Barciński, T., Beck, T., Behnke, T., Berglund, M., Bertini, I., Bieda, M., Binczyk, P., Busch, M.-D., Cacovean, A., Capria, M.T., Carr, C., Castro Marín, J.M., Ceriotti, M., Chioetto, P., Chuchra-Konrad, A., Cocola, L., Colin, F., Crews, C., Cripps, V., Cupido, E., Dassatti, A., Davidsson, B.J.R., De Roche, T., Deca, J., Del Togno, S., Dhooghe, F., Donaldson Hanna, K., Eriksson, A., Fedorov, A., Fernández-Valenzuela, E., Ferretti, S., Floriot, J., Frassetto, F., Fredriksson, J., Garnier, P., Gaweł, D., Génot, V., Gerber, T., Glassmeier, K.-H., Granvik, M., Grison, B., Gunell, H., Hachemi, T., Hagen, C., Hajra, R., Harada, Y., Hasiba, J., Haslebacher, N., Herranz De La Revilla, M.L., Hestroffer, D., Hewagama, T., Holt, C., Hviid, S., Iakubivskyi, I., Inno, L., Irwin, P., Ivanovski, S., Jansky, J., Jernej, I., Jeszenszky, H., Jiménez, J., Jorda, L., Kama, M., Kameda, S., Kelley, M.S.P., Klepacki, K., Kohout, T., Kojima, H., Kowalski, T., Kuwabara, M., Ladno, M., Laky, G., Lammer, H., Lan, R., Lavraud, B., Lazzarin, M., Le Duff, O., Lee, Q.-M., Lesniak, C., Lewis, Z., Lin, Z.-Y., Lister, T., Lowry, S., Magnes, W., Markkanen, J., Martinez Navajas, I., Martins, Z., Matsuoka, A., Matyjasiak, B., Mazelle, C., Mazzotta Epifani, E., Meier, M., Michaelis, H., Micheli, M., Migliorini, A., Millet, A.-L., Moreno, F., Mottola, S., Moutounaick, B., Muinonen, K., Müller, D.R., Murakami, G., Murata, N., Myszka, K., Nakajima, S., Nemeth, Z., Nikolajev, A., Nordera, S., Ohlsson, D., Olesk, A., Ottacher, H., Ozaki, N., Oziol, C., Patel, M., Savio Paul, A., Penttilä, A., Pernechele, C., Peterson, J., Petraglio, E., Piccirillo, A.M., Plaschke, F., Polak, S., Postberg, F., Proosa, H., Protopapa, S., Puccio, W., Ranvier, S., Raymond, S., Richter, I., Rieder, M., Rigamonti, R., Ruiz Rodriguez, I., Santolik, O., Sasaki, T., Schrödter, R., Shirley, K., Slavinskis, A., Sodor, B., Soucek, J., Stephenson, P., Stöckli, L., Szewczyk, P., Troznai, G., Uhlir, L., Usami, N., Valavanoglou, A., Vaverka, J., Wang, W., Wang, X.-D., Wattieaux, G., Wieser, M., Wolf, S., Yano, H., Yoshikawa, I., Zakharov, V., Zawistowski, T., Zuppella, P., Rinaldi, G., Ji, H., 2024. The comet interceptor mission. Space Sci. Rev. (ISSN: 1572-9672) 220 (1), 9. http://dx.doi.org/10.1007/s11214-023-01035-0.

Jones, T.J., Stark, D., Woodward, C.E., Kelley, M.S., Kolokolova, L., Clemens, D., Pinnick, A., 2008. Evidence of fragmenting dust particles from near-simultaneous optical and near-infrared photometry and polarimetry of comet 73P/schwassmann-Wachmann 3. Astron. J. 135 (4), 1318. http://dx.doi.org/10.1088/0004-6256/135/4/1318.

Jorda, L., Gaskell, R., Capanna, C., Hviid, S., Lamy, P., Ďurech, J., Faury, G., Groussin, O., Gutiérrez, P., Jackman, C., Keihm, S.J., Keller, H.U., Knollenberg, J., Kührt, E., Marchi, S., Mottola, S., Palmer, E., Schloerb, F.P., Sierks, H., Vincent, J.-B., A'Hearn, M.F., Barbieri, C., Rodrigo, R., Koschny, D., Rickman, H., Barucci, M.A., Bertaux, J.L., Bertini, I., Cremonese, G., Da Deppo, V., Davidsson, B., Debei, S., De Cecco, M., Fornasier, S., Fulle, M., Güttler, C., Ip, W.-H., Kramm, J., Küppers, M., Lara, L.M., Lazzarin, M., Lopez Moreno, J.J., Marzari, F., Naletto, G., Oklay, N., Thomas, N., Tubiana, C., Wenzel, K.-P., 2016. The global shape, density and rotation of comet 67P/Churyumov-Gerasimenko from preperihelion Rosetta/OSIRIS observations. Icarus (ISSN: 0019-1035) 277, 257–278. http://dx.doi.org/10.1016/j.icarus.2016.05.002, URL https://www.sciencedirect.com/science/article/pii/S0019103516301385.

Jorden, P., Jerram, P., Fryer, M., Stefanov, K., 2017. e2v CMOS and CCD sensors and systems for astronomy. J. Instrum. 12 (07), C07008. http://dx.doi.org/10.1088/1748-0221/12/07/C07008.

Kearsley, A.T., Borg, J., Graham, G.A., Burchell, M.J., Cole, M.J., Leroux, H., Bridges, J.C., Hörz, F., Wozniakiewicz, P.J., Bland, P.A., Bradley, J.P., Dai, Z.R., Teslich, N., See, T., Hoppe, P., Heck, P.R., Huth, J., Stadermann, F.J., Floss, C., Marhas, K., Stephan, T., Leitner, J., 2008. Dust from comet wild 2: Interpreting particle size, shape, structure, and composition from impact features on the stardust aluminum foils. Meteorit. Planet. Sci. 43 (1–2), 41–73. http://dx.doi.org/10.1111/j.1945-5100.2008.tb00609.x, URL https://onlinelibrary.wiley.com/doi/abs/10.1111/j.1945-5100.2008.tb00609.x.

Keller, H.U., Barbieri, C., Lamy, P., Rickman, H., Rodrigo, R., Wenzel, K.P., Sierks, H., A'Hearn, M.F., Angrilli, F., Angulo, M., Bailey, M.E., Barthol, P., Barucci, M.A., Bertaux, J.L., Bianchini, G., Boit, J.L., Brown, V., Burns, J.A., Büttner, I., Castro, J.M., Cremonese, G., Curdt, W., Deppo, V.D., Debei, S., Cecco, M.D., Dohlen, K., Fornasier, S., Fulle, M., Germerott, D., Gliem, F., Guizzo, G.P., Hviid, S.F., Ip, W.H., Jorda, L., Koschny, D., Kramm, J.R., Kührt, E., Küppers, M., Lara, L.M., Llebaria, A., López, A., López-Jimenez, A., López-Moreno, J., Meller, R., Michalik, H., Michelena, M.D., Müller, R., Naletto, G., Origné, A., Parzianello, G., Pertile, M., Quintana, C., Ragazzoni, R., Ramous, P., Reiche, K.U., Reina, M., Rodríguez, J., Rousset, G., Sabau, L., Sanz, A., Sivan, J.P., Stöckner, K., Tabero, J., Telljohann, U., Thomas, N., Timon, V., Tomasch, G., Wittrock, T., Zaccariotto, M., 2007. OSIRIS

the scientific camera system onboard Rosetta. Space Sci. Rev. 128 (1–4), 433–506. http://dx.doi.org/10.1007/s11214-006-9128-4.

Kerker, M., Wang, D.-S., Giles, C.L., 1983. Electromagnetic scattering by magnetic spheres. J. Opt. Soc. Am. 73 (6), 765–767. http://dx.doi.org/10.1364/JOSA.73.000765, URL https://opg.optica.org/abstract.cfm?URI=josa-73-6-765.

Kramer, T., Noack, M., Baum, D., Hege, H.-C., Heller, E.J., 2018. Dust and gas emission from cometary nuclei: the case of comet 67P/Churyumov–Gerasimenko. Adv. Phys.: X 3 (1), 1404436. http://dx.doi.org/10.1080/23746149.2017.1404436.

Langland-Shula, L.E., Smith, G.H., 2011. Comet classification with new methods for gas and dust spectroscopy. Icarus (ISSN: 0019-1035) 213 (1), 280–322. http://dx.doi.org/10.1016/j.icarus.2011.02.007, URL https://www.sciencedirect.com/science/article/pii/S001910351100056X.

Lara, L.M., Schulz, R., Stüwe, J.A., Tozzi, G.P., 2001. Activity of comet tabur (C/1996 Q1) during september 12–17, 1996. Icarus (ISSN: 0019-1035) 150 (1), 124–139. http://dx.doi.org/10.1006/icar.2000.6547, URL https://www.sciencedirect.com/science/article/pii/S0019103500965473.

Lin, Z.-Y., Lara, L.M., Vincent, J.B., Ip, W.-H., 2012. Physical studies of 81P/wild 2 from the last two apparitions. Astron. Astrophys. 537, A101. http://dx.doi.org/10.1051/0004-6361/201116848.

Lisse, C.M., A'Hearn, M.F., Farnham, T.L., Groussin, O., Meech, K.J., Fink, U., Schleicher, D.G., 2005. The coma of comet 9P/Tempel 1. Space Sci. Rev. 117 (1–2), 161–192. http://dx.doi.org/10.1007/s11214-005-3384-6.

Mannel, T., Bentley, M.S., Schmied, R., Jeszenszky, H., Levasseur-Regourd, A.C., Romstedt, J., Torkar, K., 2016. Fractal cometary dust – A window into the early solar system. Mon. Not. R. Astron. Soc. (ISSN: 0035-8711) 462 (Suppl1), S304–S311. http://dx.doi.org/10.1093/mnras/stw2898.

Markkanen, J., Agarwal, J., 2019. Scattering, absorption, and thermal emission by large cometary dust particles: Synoptic numerical solution. Astron. Astrophys. 631, http://dx.doi.org/10.1051/0004-6361/201936235.

Marschall, R., Skorov, Y., Zakharov, V., Rezac, L., Gerig, S., Christou, C., Dadzie, S.K., Migliorini, A., Rinaldi, G., Agarwal, J., Vincent, J.-B., Kappel, D., 2020. Cometary comae-surface links. Space Sci. Rev. (ISSN: 1572-9672) 216 (8), 130. http://dx.doi.org/10.1007/s11214-020-00744-0.

Marschall, R., Zakharov, V., Tubiana, C., Kelley, M.S.P., van Damme, C.C., Snodgrass, C., Jones, G.H., Ivanovski, S.L., Postberg, F., Vincenzo, V.D., Vincent, J.-B., Muñoz, La Forgia, F., Levasseur-Regourd, A.-C., the Comet Interceptor Team, 2022. Determining the dust environment of an unknown comet for a spacecraft flyby: The case of ESA´s comet interceptor mission. Astron. Astrophys. 666, A151. http://dx.doi.org/10.1051/0004-6361/202243648.

Matrajt, G., Ito, M., Wirick, S., Messenger, S., Brownlee, D.E., Joswiak, D., Flynn, G., Sandford, S., Snead, C., Westphal, A., 2008. Carbon investigation of two stardust particles: A TEM, NanoSIMS, and XANES study. Meteorit. Planet. Sci. 43 (1–2), 315–334. http://dx.doi.org/10.1111/j.1945-5100.2008.tb00625.x, URL https://onlinelibrary.wiley.com/doi/abs/10.1111/j.1945-5100.2008.tb00625.x.

Mazzotta Epifani, E., Palumbo, P., Capria, M.T., Cremonese, G., Fulle, M., Colangeli, L., 2007. The distant activity of short-period comets – I. Mon. Not. R. Astron. Soc. (ISSN: 0035-8711) 381 (2), 713–722. http://dx.doi.org/10.1111/j.1365-2966.2007.12181.x.

Mazzotta Epifani, E., Perna, D., Di Fabrizio, L., Dall´Ora, M., Palumbo, P., Snodgrass, C., Licandro, J., Della Corte, V., Tozzi, G.P., 2014. Observational results for eight long-period comets observed far from the sun. Astron. Astrophys. 561, A6. http://dx.doi.org/10.1051/0004-6361/201321290.

McDonnell, J.A.M., Evans, G.C., Evans, S.T., Alexander, W.M., Burton, W.M., Firth, J.G., Bussoletti, E., Grard, R.J.L., Hanner, M.S., Sekanina, Z., Stevenson, T.J., Turner, R.F., Weishaupt, U., Wallis, M.K., Zarnecki, J.C., 1987. The dust distribution within the inner coma of comet P/Halley 1982i - encounter by Giotto's impact detectors. Astron. Astrophys. 187 (1–2), 719–741.

Merouane, S., Zaprudin, B., Stenzel, O., Langevin, Y., Altobelli, N., Della Corte, V., Fischer, H., Fulle, M., Hornung, K., Silén, J., Ligier, N., Rotundi, A., Ryno, J., Schulz, R., Hilchenbach, M., Kissel, J., the COSIMA Team, 2016. Dust particle flux and size distribution in the coma of 67P/Churyumov-Gerasimenko measured in situ by the COSIMA instrument on board Rosetta. Astron. Astrophys. 596, A87. http://dx.doi.org/10.1051/0004-6361/201527958.

Mishchenko, M.I., 1991. Light scattering by randomly oriented axially symmetric particles. J. Opt. Soc. Amer. A 8 (6), 871–882. http://dx.doi.org/10.1364/JOSAA.8.000871, URL https://opg.optica.org/josaa/abstract.cfm?URI=josaa-8-6-871.

Mishchenko, M.I., 2007. Electromagnetic scattering by a fixed finite object embedded in an absorbing medium. Opt. Express 15 (20), 13188–13202. http://dx.doi.org/10.1364/OE.15.013188, URL https://opg.optica.org/oe/abstract.cfm?URI=oe-15-20-13188.

Mishchenko, M.I., Travis, L.D., Mackowski, D.W., 1996. T-matrix computations of light scattering by nonspherical particles: A review. J. Quant. Spectrosc. Radiat. Transfer (ISSN: 0022-4073) 55 (5), 535–575. http://dx.doi.org/10.1016/0022-4073(96)00002-7, URL https://www.sciencedirect.com/science/article/pii/0022407396000027, Light Scattering by Non-Spherical Particles.

Moosmuller, H., Ogren, J., 2017. Parameterization of the aerosol upscatter fraction as function of the backscatter fraction and their relationships to the asymmetry parameter for radiative transfer calculations. Atmosphere 2017, http://dx.doi.org/10.3390/atmos8080133.

Moosmüller, H., Sorensen, C.M., 2018. Small and large particle limits of single scattering albedo for homogeneous, spherical particles. J. Quant. Spectrosc. Radiat. Transfer (ISSN: 0022-4073) 204, 250–255. http://dx.doi.org/10.1016/j.jqsrt.2017.09.029, URL https://www.sciencedirect.com/science/article/pii/S0022407317305861.

Moreels, G., Clairemidi, J., Parisot, J.P., Zucconi, J.M., Bertaux, J.L., Blamont, J.E., Hersé, M., Krasnopolsky, V.A., Moroz, V.I., Krysko, A.A., Tkachuk, A.Y., Gogoshev, M., Gogosheva, T., Werner, R., Spasov, S., 1988. Spectrophotometry of comet P/Halley at wavelengths 275—710 nm from vega 2. In: Grewing, M., Praderie, F., Reinhard, R. (Eds.), Exploration of Halley's Comet. Springer Berlin Heidelberg, Berlin, Heidelberg, ISBN: 978-3-642-82971-0, pp. 551–559.

Moteki, N., 2016. Gmie cpp. https://github.com/nmoteki/gmie_cpp,

Opitom, C., Snodgrass, C., Fitzsimmons, A., Jehin, E., Manfroid, J., Tozzi, G.P., Faggi, S., Gillon, M., 2017. Ground-based monitoring of comet 67P/Churyumov–Gerasimenko gas activity throughout the Rosetta mission. Mon. Not. R. Astron. Soc. (ISSN: 0035-8711) 469 (Suppl_2), S222–S229. http://dx.doi.org/10.1093/mnras/stx1591.

Ott, T., Drolshagen, E., Koschny, D., Güttler, C., Tubiana, C., Frattin, E., Agarwal, J., Sierks, H., Bertini, I., Barbieri, C., Lamy, P.I., Rodrigo, R., Rickman, H., A'Hearn, M.F., Barucci, M.A., Bertaux, J.-L., Boudreault, S., Cremonese, G., Da Deppo, V., Davidsson, B., Debei, S., De Cecco, M., Deller, J., Feller, C., Fornasier, S., Fulle, M., Geiger, B., Gicquel, A., Groussin, O., Gutiérrez, P.J., Hofmann, M., Hviid, S.F., Ip, W.-H., Jorda, L., Keller, H.U., Knollenberg, J., Kovacs, G., Kramm, J.R., Kührt, E., Küppers, M., Lara, L.M., Lazzarin, M., Lin, Z.-Y., López-Moreno, J.J., Marzari, F., Mottola, S., Naletto, G., Oklay, N., Pajola, M., Shi, X., Thomas, N., Vincent, J.-B., Poppe, B., 2017. Dust mass distribution around comet 67P/Churyumov–Gerasimenko determined via parallax measurements using Rosetta's OSIRIS cameras. Mon. Not. R. Astron. Soc. (ISSN: 0035-8711) 469 (suppl2), S276–S284. http://dx.doi.org/10.1093/mnras/stx1419.

Pollack, J.B., Cuzzi, J.N., 1980. Scattering by nonspherical particles of size comparable to a wavelength: A new semi-empirical theory and its application to tropospheric aerosols. J. Atmos. Sci. 37 (4), 868–881. http://dx.doi.org/10.1175/1520-0469(1980)037<0868:SBNPOS>2.0.CO;2.

Reinhard, R., 1997. Giotto mission. In: Encyclopedia of Planetary Science. Springer Netherlands, Dordrecht, ISBN: 978-1-4020-4520-2, pp. 274–279. http://dx.doi.org/10.1007/1-4020-4520-4_1560.

Rinaldi, G., Della Corte, V., Fulle, M., Capaccioni, F., Rotundi, A., Ivanovski, S.L., Bockelée-Morvan, D., Filacchione, G., D'Aversa, E., Capria, M.T., Tozzi, G.P., Erard, S., Leyrat, C., Palomba, E., Longobardo, A., Ciarniello, M., Taylor, F., Mottola, S., Salatti, M., 2017. Cometary coma dust size distribution from in situ IR spectra. Mon. Not. R. Astron. Soc. (ISSN: 0035-8711) 469 (suppl2), S598–S605. http://dx.doi.org/10.1093/mnras/stx1873.

Rosenbush, V.K., Ivanova, O.V., Kiselev, N.N., Kolokolova, L.O., Afanasiev, V.L., 2017. Spatial variations of brightness, colour and polarization of dust in comet 67P/Churyumov–Gerasimenko. Mon. Not. R. Astron. Soc. (ISSN: 0035-8711) 469 (suppl2), S475–S491. http://dx.doi.org/10.1093/mnras/stx2003.

Rucks, M., Ye, C., Sklute, E., Arnold, J., DiFrancesco, N., Glotch, T., 2022. Visible to mid-infrared optical constants of orthopyroxenes. Earth Space Sci. 9, http://dx.doi.org/10.1029/2021EA002104.

Sárneczky, K., Szabó, G.M., Csák, B., Kelemen, J., Marschalkó, G., Pál, A., Szakáts, R., Szalai, T., Szegedi-Elek, E., Székely, P., Vida, K., Vinkó, J., Kiss, L.L., 2016. Activity of 50 long-period comets beyond 5.2 AU. Astron. J. 152 (6), 220. http://dx.doi.org/10.3847/0004-6256/152/6/220.

Schulz, R., Owens, A., Rodriguez-Pascual, P.M., Lumb, D., Erd, C., Stüwe, J.A., 2006. Detection of water ice grains after the DEEP IMPACT onto comet 9P/Tempel 1. Astron. Astrophys. 448 (3), L53–L56. http://dx.doi.org/10.1051/0004-6361:200600003.

Shugarov, A.S., 2020. The prospects of modern CMOS and CCD detectors for wide field telescopes. INASAN Sci. Rep. 5, 236–242. http://dx.doi.org/10.26087/INASAN.2020.5.5.003.

Sivaraman, K.R., Babu, G.S.D., Shylaja, B.S., Rajamohan, R., 1988. Spectrophotometry of comet P/Halley. In: Grewing, M., Praderie, F., Reinhard, R. (Eds.), Exploration of Halley's Comet. Springer Berlin Heidelberg, Berlin, Heidelberg, ISBN: 978-3-642-82971-0, pp. 543–550.

Snodgrass, C., Jones, G.H., 2019. The European space agency's comet interceptor lies in wait. Nature Commun. (ISSN: 2041-1723) 10 (1), 5418. http://dx.doi.org/10.1038/s41467-019-13470-1.

Stagg, B., Charalampopoulos, T., 1993. Refractive indices of pyrolytic graphite, amorphous carbon, and flame soot in the temperature range 25° to 600° C. Combust. Flame (ISSN: 0010-2180) 94 (4), 381–396. http://dx.doi.org/10.1016/0010-2180(93)90121-I, URL https://www.sciencedirect.com/science/article/pii/001021809390121I.

Thomas, N., Keller, H.U., 1990. Interpretation of the inner coma observations of comet P/Halley by the halley multicolour camera. Ann. Geophys. 8, 147–165.

Tubiana, C., Snodgrass, C., Bertini, I., Mottola, S., Vincent, J.-B., Lara, L., Fornasier, S., Knollenberg, J., Thomas, N., Fulle, M., Agarwal, J., Bodewits, D., Ferri, F., Güttler, C., Gutierrez, P.J., La Forgia, F., Lowry, S., Magrin, S., Oklay, N., Pajola, M., Rodrigo, R., Sierks, H., A'Hearn, M.F., Angrilli, F., Barbieri, C., Barucci, M.A., Bertaux, J.-L., Cremonese, G., Da Deppo, V., Davidsson, B., De Cecco, M., Debei, S., Groussin, O., Hviid, S.F., Ip, W., Jorda, L., Keller, H.U., Koschny, D., Kramm, R., Kührt, E., Küppers, M., Lazzarin, M., Lamy, P.L., Lopez Moreno, J.J., Marzari, F., Michalik, H., Naletto, G., Rickman, H., Sabau, L., Wenzel, K.-P.,

2015. 67P/Churyumov-Gerasimenko: Activity between March and June 2014 as observed from Rosetta/OSIRIS. Astron. Astrophys. 573, A62. http://dx.doi.org/10.1051/0004-6361/201424735.

Voitko, A., Zubko, E., Ivanova, O., Husárik, M., Videen, G., 2024. Dust color variations of comet C/2016 M1 (PanSTARRS). Icarus (ISSN: 0019-1035) 411, 115967. http://dx.doi.org/10.1016/j.icarus.2024.115967, URL https://www.sciencedirect.com/science/article/pii/S0019103524000253.

Voitko, A., Zubko, E., Ivanova, O., Luk'yanyk, I., Kochergin, A., Husárik, M., Videen, G., 2022. Color variations of comet 29P/Schwassmann–Wachmann 1 in 2018. Icarus (ISSN: 0019-1035) 388, 115236. http://dx.doi.org/10.1016/j.icarus.2022.115236, URL https://www.sciencedirect.com/science/article/pii/S0019103522003293.

Weiler, M., Rauer, H., Knollenberg, J., Jorda, L., Helbert, J., 2003. The dust activity of comet C/1995 O1 (Hale-Bopp) between 3 AU and 13 AU from the Sun*. Astron. Astrophys. 403 (1), 313–322. http://dx.doi.org/10.1051/0004-6361:20030289.

Wooden, D.H., Ishii, H.A., Zolensky, M.E., 2017. Cometary dust: the diversity of primitive refractory grains. Philos. Trans. Ser. A, Math., Phys., Eng. Sci. 375, URL https://api.semanticscholar.org/CorpusID:21386889.

Woodward, C.E., Wooden, D.H., Harker, D.E., Kelley, M.S.P., Russell, R.W., Kim, D.L., 2021. The coma dust of comet C/2013 US10 (Catalina): A window into carbon in the solar system. Planet. Sci. J. 2 (1), 25. http://dx.doi.org/10.3847/PSJ/abca3e.

Yamamoto, T., Ashihara, O., 1985. Condensation of ice particles in the vicinity of a cometary nucleus. Astron. Astrophys. 152 (2), L17–L20.

Zakharov, V.V., Rodionov, A.V., Fulle, M., Ivanovski, S.L., Bykov, N.Y., Della Corte, V., Rotundi, A., 2021a. Practical relations for assessments of the gas coma parameters. Icarus (ISSN: 0019-1035) 354, 114091. http://dx.doi.org/10.1016/j.icarus.2020.114091, URL https://www.sciencedirect.com/science/article/pii/S0019103520304371.

Zakharov, V.V., Rotundi, A., Della Corte, V., Fulle, M., Ivanovski, S.L., Rodionov, A.V., Bykov, N.Y., 2021b. On the similarity of dust flows in the inner coma of comets. Icarus (ISSN: 0019-1035) 364, 114476. http://dx.doi.org/10.1016/j.icarus.2021.114476, URL https://www.sciencedirect.com/science/article/pii/S0019103521001561.